**International Journal of Applied and Natural Sciences**
ISSN: 3005-3471
DOI: 10.61424/ijans
Journal Homepage: www.bluemarkpublishers.com/index.php/IJANS

IJANS
BLUEMARK PUBLISHERS

**| RESEARCH ARTICLE**

# Optimizing Process Parameters for ASTM A36 Steel Welding with a Locally Manufactured Arc Welding Machine

**Vincent Chukwuemeka Ezechukwu[1] ✉ Iromaka Ijeomanta Chidi[2] and Kingsley Chinedu Owuama[3]**
*[123]Doctor of Philosophy, Department of Mechanical Engineering, Chukwuemeka Odumegwu Ojukwu University, Anambra State, Nigeria*
**Corresponding Author:** Vincent Chukwuemeka Ezechukwu, **E-mail**: vc.ezechukwu@coou.edu.ng

**| ABSTRACT**
In many different industries, welding is a common joining technique. However, due to a lack of finance, tiny fabrication businesses in Nigeria frequently use simple manual arc welding equipment. Although these systems enable necessary joining activities, their erratic performance over time degrades output and quality. Welds are unreliable and may need to be redone if the process parameters are not systematically understood. This also restricts the thickness of materials that may be employed. Through experiment design, this study sought to optimize the characteristics of a manually operated shielded metal arc welding (SMAW) machine. Current, voltage, electrode diameter, and travel speed were found to be important adjustable parameters. To examine how changes in these variables affect the results of weld quality, an experimental design was created. The manual SMAW machine's ideal parameters were determined to be 46.498 amps of current, 28.662 volts of voltage, 2.920 mm of electrode diameter, and 100 mm/min of travel speed. The anticipated tensile shear strength at these levels was 502.362 MPa, the micro hardness was 437.736 kgf/mm2, and the weld bead width was 6.124 mm. When compared to the machine's initial capabilities, performance under optimal conditions demonstrated increases in productivity, dependability, and defect reduction. To assist Nigeria's industrialization objectives, local technical skills can be sustainably developed through the methodical improvement of current resources.

**| KEYWORDS**
ASTM A36 steel, welding, microstructure, response surface methodology, hardness.

**| ARTICLE INFORMATION**
**ACCEPTED:** 15 November 2024 **PUBLISHED:** 21 December 2024 **DOI:** 10.61424/ijans.v2.i2.163

## 1. Introduction
In several sectors, such as industrial, automotive, and construction, ASTM A36 steel welding has been essential to structural production. A36 is a low-carbon steel with exceptional weldability, which makes it a popular option for many applications where formability and strength are essential [Chidambaresh, 2023]. However, the cost-effectiveness and structural integrity of the finished goods are greatly impacted by the quality and efficiency of welding operations. Arc welding has been popular in small-scale enterprises and developing countries because of its affordability and adaptability, especially when done with locally made equipment. For these machines, it is essential to optimize the welding parameters in order to guarantee that the welds fulfill performance criteria and industry standards [Elahi, 2023]. ASTM A36 steel is appropriate for a variety of structural applications due to its mechanical characteristics, which include its tensile strength ranging from 400 to 550 MPa and yield strength of 250 MPa [Ezechukwu, 2020]. To preserve or improve the material's performance, welding parameters must be carefully

controlled because the procedure can drastically change these qualities [Ezechukwu, 2020]. The effects of current, voltage, and travel speed on the tensile strength of A36 steel welds were examined using a factorial design in one of the first studies in this area. The results obtained established the foundation for further optimization research and demonstrated the important interplay between these elements. [Vietanti, 2021] The results established the foundation for further optimization research and demonstrated the important connection between these elements. To improve the welding settings for A36 steel, response surface methodology (RSM) was developed. The study showed how systematic parameter adjustment can lead to increased weld quality and productivity [Martínez-Conesa, 2017]. The microstructure and mechanical characteristics of A36 steel welds have been demonstrated to be significantly impacted by thermal management during welding, including preheat and interpass temperature control [Ezechukwu, 2024]. The application of machine learning and artificial intelligence techniques to welding parameter optimization has gained popularity in recent years. According to Braide *et al.* [2023], neural networks can forecast the best welding parameters for A36 steel with encouraging accuracy and efficiency outcomes.

## 2. Materials and Method

### *2.1 Materials*

A manually operated shielded metal arc welding (SMAW) system, manufactured in-house at the OPERATECH Engineering Workshop in Coal Camp, Enugu, Nigeria, served as the welding apparatus for this study. The base metal selected for this study is mild steel due to its widespread industrial usage and suitability for manual welding processes like SMAW. Specifically, ASTM A36 steel sheets will be used, which are widely used in general fabrication, structural, and pressure vessel applications.

### *2.2 Method*

A 230V/60Hz step-down transformer that is connected to the national grid serves as the power supply. Through the use of a silicon-controlled rectifier module, it transforms the mains supply voltage from AC to DC and produces the necessary welding voltages, which fall between 20 and 30V. At 30% duty cycle, the transformer's rated output capacity is 60A. Flexible guiding tubes powered by friction feed rollers with adjustable speed and a low-torque DC motor with an integrated gearbox feed electrode/filler wire from a spool mounted on the machine. This offers wire feeding rates between 1 and 5 meters per minute. Welding voltage is monitored by a small voltage sensor circuit. The torch handle, which contains water-cooled copper contact tips and nozzles of sizes 1.6-3.2mm for various electrode diameters, receives electricity from the power source via a locally constructed 60A insulated copper cable assembly. The handle of the torch has a trigger switch and an adjustable wire cutter. Crocodile clips are used to hold test plates firmly in place while welding and the earth-connected work clamp is a sturdy copper bus bar set on an insulated platform. Using movable knobs, the front panel regulates the welding current between 20 and 60A, the voltage between 20 and 30V, and the wire feed speed between 1 and 5 meters per minute. The welding process is managed by power ON/OFF and trigger switches, with feedback from a voltmeter and an ammeter. Although the torch uses an external pump and radiator to circulate water, the parts are fixed to a sturdy welded steel frame with a passive cooling system utilizing natural convection. Mobility is made possible by caster wheels, and maintenance access is made possible by detachable panels.

Figure 1: pictorial view of the locally made manually operated shielded metal arc welding (SMAW) system

### *2.2.1 Process parameters optimized*

Welding process parameters are the controllable variables that influence weld bead formation and properties. Careful regulation of these is critical to ensure repeatable quality. For manual SMAW, key adjustable parameters include welding current, voltage, electrode diameter, and travel speed.

### *2.2.1 Welding Current*

The amount of heat input and the degree of weld penetration are determined by the welding current. It is among the most important factors affecting the mechanical characteristics and geometry of the weld pool. The front panel knob on this machine allows you to adjust the current between 20 and 60 amps. Incomplete fusion occurs at lower currents because there is not enough heat for joint melting. Wider beads with less strength because of coarse grains and more splatter are the results of higher currents that are over the ideal range. The machine's 60A rated capacity may limit the scope of optimization.

### *2.2.2 Welding Voltage*

Arc stability and heat input are affected by welding voltage. Based on wire feed and current settings, the inbuilt SCR feedback circuitry mainly regulates it on its own. However, the voltage knob allows for minor modifications between 20 and 30 volts. Very low voltages cause the arc to become unstable, whereas higher voltages enhance heat input but impair arc control. It is necessary to assess the combined effects of voltage fluctuations on penetration and bead profile because they have an impact on current to some degree. The fundamental design of the power source may cause operating restrictions to appear.

### *2.2.3 Diameter of the Electrode*

The impact of various electrode sizes, which range from 2 to 3.2 mm, on the properties of the weld pool and parameter sensitivity will be examined. Although wider, coarser beads are more susceptible to cracking from increasing heat, larger diameters improve penetration. Although they run the danger of insufficient fusion, thinner electrodes produce narrower beads that are appropriate for thin materials. Material thickness compatibility is crucial.

### *2.2.4 Travel Speed*

Heat input at the joint is dominated by travel speed or weld advancement rate in an inverse relationship. Faster welding transfers less heat than slower welding, which permits more heat input. Because of the high heat, very slow or halted welding runs the danger of centerline melting faults. Unevenness, cold lap, and partial fusion might result from traveling too quickly. Evaluation is necessary to reach the ideal interactive speed range.

### *2.2.5 Material Preparation*

Four lap joint specimens were created using eight mild steel plates, two for each joint, each measuring 100 x 25 x 4 mm in thickness. To guarantee uniform chemical composition and microstructure, the plates were guillotine-sheared from a single ASTM A36 sheet. A vertical milling machine was used to face mill the edges that need to be

welded in order to eliminate any rolled-in stresses or surface flaws caused by the shearing process. For a rigid fit-up of the joint, milling will create flawlessly flat, burr-free faying surfaces. The plates went through a degreasing procedure after milling to remove any remaining grease from handling or lubricating fluids used during production. To dissolve and remove any impurities, a chemical degreaser was liberally applied and scrubbed with a wire brush. After that, clean water was used to completely rinse the plates. During welding, degreasing removes contaminants and encourages appropriate wetting of the joint surfaces. By preventing impurities from becoming trapped in the weld pool and weakening the subsequent mechanical qualities, it prevents welding errors.

### *2.2.6 Edge Preparation*

As manual SMAW is being used with no advanced joint preparation, a simple square groove weld joint configuration will be adopted. Using a hand-held Marking Table, pencil lines will be scribed 10mm from the plate edges, demarcating the weld area boundaries. The weld preparation is purposefully kept basic to realistically mimic typical Nigerian workshop conditions of manually preparing edges without sophisticated machinery. While beveling or V-grooves promote greater penetration and fusion, such complexity is rarely practical or affordable for many local operators.

## *2.3 Experimental Set-Up*

### *2.3.1 Design and Layout*

#### *2.3.1.1 Trial Run and Modifications*

A practice run will be carried out to confirm and adjust the process as needed before starting the experimental welds. Trial and error will be used to confirm the machine's operational current and voltage limits once more. As seen, minor adjustments will be performed, such as strengthening loose connections. The machine is prepared to carry out the specified series of welding tests exactly as intended in order to produce statistically significant results after satisfactory results have been obtained.

#### *2.3.1.2 Welding Procedure*

For every experimental run, welding will commence upon triggering the torch switch. The electrode will be held at a consistent angle and contact tip-to-work distance of 10mm. While welding linearly along the 50mm joint length, care will be taken to maintain a constant travel speed using a metronome beat. Shielding gas will continue flowing for 2 minutes post-welding to allow proper weld solidification. Each weld will be visually inspected for defects and integrity before commencing the next run as per the design matrix sequence.

#### *2.3.1.3 Design of Experiment*

To investigate the impacts and interplay of welding process parameters on weld quality output responses, a methodical approach known as design of experiments (DOE) will be used. In order to improve three product features that are measured as results from a design experiment, the welding performance was examined in this study.

1. Response 1: Weld bead geometry(width) (mm)
2. Response 2: Microhardness values (kgf/mm2)
3. Response 3: Tensile shear strength (MPa)

Again, four primary factors that affect the performance of the dryer vary as shown:

1. $40 \leq A$ (Current) $\leq 60$ (A) ….@ (3 levels)
2. $25 \leq B$ (Voltage) $\leq 30$ (V) ….@ (3 levels)
3. $2 \leq C$ (Electrode diameter) $\leq 3.2$ (mm) ….@ (3 levels)
4. 60 cm/min $\leq D$ (Travel speed) $\leq 100$ cm/min ….@ (3 levels)

The DESIGN EXPERT SOFTWARE 13.0 was used for the experiment. In order to develop a flexible design structure that could support irregular (constrained) regions, categorical components, and bespoke models, the optimal (custom) design was used. A selection criterion selected during the build defined the runs. The experiment formulation produced by the software is displayed in Table 1. This will act as a roadmap for this research.

Table 1: DESIGN OF EXPERIMENT FORMULATION

| | Factor 1 | Factor 2 | Factor 3 | Factor 4 | Response 1 | Response 2 | Response 3 |
|---|---|---|---|---|---|---|---|
| Run | A: Current | B: Voltage | C: Electrode diameter | D: Travel speed | Weld bead geometry | Microhardness values | Tensile shear strength |
| | A | V | mm | cm/min | mm | kgf/mm$^2$ | MPa |
| 1 | 40 | 30 | 3.2 | 75 | | | |
| 2 | 40 | 25 | 3.2 | 100 | | | |
| 3 | 50 | 30 | 3.2 | 60 | | | |
| 4 | 60 | 30 | 2 | 100 | | | |
| 5 | 60 | 27 | 2 | 75 | | | |
| 6 | 40 | 25 | 2.5 | 75 | | | |
| 7 | 50 | 25 | 2.5 | 60 | | | |
| 8 | 60 | 30 | 2 | 60 | | | |
| 9 | 50 | 27 | 2.5 | 100 | | | |
| 10 | 60 | 27 | 3.2 | 60 | | | |
| 11 | 60 | 25 | 2 | 60 | | | |
| 12 | 40 | 30 | 2.5 | 100 | | | |
| 13 | 60 | 30 | 3.2 | 100 | | | |
| 14 | 50 | 27 | 2.5 | 100 | | | |
| 15 | 50 | 27 | 3.2 | 75 | | | |
| 16 | 50 | 27 | 2 | 60 | | | |
| 17 | 40 | 27 | 2.5 | 60 | | | |
| 18 | 60 | 25 | 3.2 | 100 | | | |
| 19 | 40 | 27 | 2 | 75 | | | |
| 20 | 50 | 30 | 2 | 75 | | | |
| 21 | 50 | 27 | 2.5 | 100 | | | |
| 22 | 60 | 30 | 2.5 | 75 | | | |
| 23 | 40 | 25 | 2 | 100 | | | |

## 3. Results and Discussion

### *3.1 Analysis Result*

A full quadratic model was used for each result in order to investigate how certain factors of manually operated shielded metal arc welding (SMAW) affect its performance under particular circumstances [Ezechukwu, 2015]. The model's excellent fit to the experimental data served as the basis for this decision. An analysis of variance (ANOVA) was then used to determine the statistical significance of these created models [Erebugha, 2024]. A regression analysis and a normal plot of residuals were performed to support the models' dependability. Table 2 presents the practical results of the trials carried out at different combinations of the chosen stove characteristics.

Table 2. Experimental Design and response results

| | Factor 1 | Factor 2 | Factor 3 | Factor 4 | Response 1 | Response 2 | Response 3 |
|---|---|---|---|---|---|---|---|
| Run | A: Current | B: Voltage | C: Electrode diameter | D: Travel speed | Weld bead geometry(width) | Microhardness values | Tensile shear strength |
| | A | V | mm | cm/min | mm | $kgf/mm^2$ | MPa |
| 1 | 40 | 30 | 3.2 | 75 | 5 | 450 | 500 |
| 2 | 40 | 25 | 3.2 | 100 | 5 | 425 | 475 |
| 3 | 50 | 30 | 3.2 | 60 | 6 | 475 | 525 |
| 4 | 60 | 30 | 2 | 100 | 4 | 400 | 450 |
| 5 | 60 | 27 | 2 | 75 | 4 | 410 | 460 |
| 6 | 40 | 25 | 2.5 | 75 | 6 | 435 | 485 |
| 7 | 50 | 25 | 2.5 | 60 | 6 | 465 | 515 |
| 8 | 60 | 30 | 2 | 60 | 6 | 480 | 530 |
| 9 | 50 | 27 | 2.5 | 100 | 6 | 445 | 495 |
| 10 | 60 | 27 | 3.2 | 60 | 7 | 470 | 520 |
| 11 | 60 | 25 | 2 | 60 | 6 | 475 | 525 |
| 12 | 40 | 30 | 2.5 | 100 | 6 | 435 | 485 |
| 13 | 60 | 30 | 3.2 | 100 | 7 | 425 | 525 |
| 14 | 50 | 27 | 2.5 | 100 | 6 | 445 | 495 |
| 15 | 50 | 27 | 3.2 | 75 | 7 | 470 | 520 |
| 16 | 50 | 27 | 2 | 60 | 6 | 480 | 530 |
| 17 | 40 | 27 | 2.5 | 60 | 6 | 435 | 485 |
| 18 | 60 | 25 | 3.2 | 100 | 7 | 470 | 520 |
| 19 | 40 | 27 | 2 | 75 | 5 | 425 | 475 |
| 20 | 50 | 30 | 2 | 75 | 6 | 475 | 525 |
| 21 | 50 | 27 | 2.5 | 100 | 6 | 445 | 495 |
| 22 | 60 | 30 | 2.5 | 75 | 7 | 470 | 520 |
| 23 | 40 | 25 | 2 | 100 | 5 | 425 | 475 |

### *3.2 Analysis of Variance (ANOVA)*

A variety of statistical models and associated estimating methods make up the analysis of variance (ANOVA). It is used to investigate differences within and between groups, particularly when analyzing group mean differences within a sample. To ascertain whether there is a significant variation in the experiment's mean results, ANOVA was used in this investigation. The ANOVA results for the weld bead geometry (width), microhardness values, and tensile shear strength values obtained from the experimental data are displayed in Tables 3, 4, and 5. These tables give information about the coefficients of the corresponding models as well as the statistical significance of the factors in question.

I: For the Weld bead geometry (width), the ANVOA for the selected factorial model is seen below:

Table 3. Analysis of Variance results for Weld bead geometry (width)

| Source | Sum of Squares | df | Mean Square | F-value | p-value | |
|---|---|---|---|---|---|---|
| **Model** | 15.42 | 17 | 0.9069 | 3.81 | 0.0727 | not significant |
| A-Current | 1.33 | 1 | 1.33 | 5.58 | 0.0645 | |
| B-Voltage | 0.4600 | 1 | 0.4600 | 1.93 | 0.2233 | |
| C-Electrode diameter | 4.03 | 1 | 4.03 | 16.92 | 0.0092 | |
| D-Travel speed | 1.50 | 2 | 0.7497 | 3.15 | 0.1303 | |
| AB | 0.0004 | 1 | 0.0004 | 0.0015 | 0.9709 | |
| AC | 5.88 | 1 | 5.88 | 24.68 | 0.0042 | |
| AD | 0.7875 | 2 | 0.3937 | 1.65 | 0.2811 | |
| BC | 0.2059 | 1 | 0.2059 | 0.8648 | 0.3951 | |
| BD | 0.0071 | 2 | 0.0036 | 0.0149 | 0.9852 | |
| CD | 2.72 | 2 | 1.36 | 5.71 | 0.0512 | |
| $A^2$ | 0.4498 | 1 | 0.4498 | 1.89 | 0.2278 | |
| $B^2$ | 0.1138 | 1 | 0.1138 | 0.4781 | 0.5201 | |
| $C^2$ | 1.66 | 1 | 1.66 | 6.97 | 0.0460 | |
| **Residual** | 1.19 | 5 | 0.2381 | | | |
| Lack of Fit | 1.19 | 3 | 0.3969 | | | |
| Pure Error | 0.0000 | 2 | 0.0000 | | | |
| **Cor Total** | 16.61 | 22 | | | | |

According to the F-value of the model, which is 3.81, there is a 7.27% chance that an F-value this high may happen by chance. P-values below 0.05 suggest that model terms such as C, AC, and C2 have a substantial role in response prediction. The predictions are not significantly impacted by the associated model terms, as indicated by P-values greater than 0.1. Since several factors have high insignificant values, the model might be improved by eliminating some of the terms using stepwise regression. If the model's adjusted R-squared is negative, it is not substantially more predictive than merely using the average. A more accurate response prediction might be possible with a higher order model. An appropriate signal is shown by the signal-to-noise ratio over 4, which is 7.117 in this case. So, this model is appropriate for navigating the design space to understand the response.

II: For the Microhardness values, the ANVOA for the selected factorial model is seen below:

Table 4. Analysis of Variance results for Microhardness values

| Source | Sum of Squares | df | Mean Square | F-value | p-value | |
|---|---|---|---|---|---|---|
| Model | 12455.53 | 17 | 732.68 | 9.72 | 0.0098 | significant |
| A-Current | 612.98 | 1 | 612.98 | 8.13 | 0.0358 | |
| B-Voltage | 231.34 | 1 | 231.34 | 3.07 | 0.1403 | |
| C-Electrode diameter | 193.73 | 1 | 193.73 | 2.57 | 0.1699 | |
| D-Travel speed | 4072.28 | 2 | 2036.14 | 27.00 | 0.0021 | |
| AB | 435.70 | 1 | 435.70 | 5.78 | 0.0613 | |
| AC | 1290.43 | 1 | 1290.43 | 17.11 | 0.0090 | |
| AD | 679.20 | 2 | 339.60 | 4.50 | 0.0761 | |
| BC | 234.99 | 1 | 234.99 | 3.12 | 0.1378 | |
| BD | 913.07 | 2 | 456.53 | 6.05 | 0.0462 | |
| CD | 1189.98 | 2 | 594.99 | 7.89 | 0.0284 | |
| $A^2$ | 1631.88 | 1 | 1631.88 | 21.64 | 0.0056 | |
| $B^2$ | 459.09 | 1 | 459.09 | 6.09 | 0.0567 | |
| $C^2$ | 265.55 | 1 | 265.55 | 3.52 | 0.1194 | |
| Residual | 377.07 | 5 | 75.41 | | | |
| Lack of Fit | 377.07 | 3 | 125.69 | | | |
| Pure Error | 0.0000 | 2 | 0.0000 | | | |
| Cor Total | 12832.61 | 22 | | | | |

The relatively large model F-value of 9.72 suggests that the model is statistically significant. There is only a 0.98% probability that an F-value this high could be due to random noise. Terms with p-values less than 0.05, such as A, D, AC, BD, CD, and A2, meaningfully contribute to predicting the response. Terms with p-values over 0.1 do not notably impact the predictions. Since some terms are highly insignificant, removing unnecessary terms via stepwise selection may enhance the model. On occasion, a higher order model could more accurately forecast the response. The signal-to-noise ratio exceeding 4, which is 11.492 in this case, demonstrates sufficient signal. Therefore, this validated model is suitable for navigating the design space to understand how the response behaves with changes in the factors.

III: For the Tensile shear strength values, the ANVOA for the selected factorial model is seen below:

Table 5. Analysis of Variance results for Tensile shear strength values

| Source | Sum of Squares | df | Mean Square | F-value | p-value | |
|---|---|---|---|---|---|---|
| **Model** | 12534.10 | 17 | 737.30 | 13.32 | 0.0048 | significant |
| A-Current | 959.36 | 1 | 959.36 | 17.33 | 0.0088 | |
| B-Voltage | 988.65 | 1 | 988.65 | 17.86 | 0.0083 | |
| C-Electrode diameter | 900.99 | 1 | 900.99 | 16.28 | 0.0100 | |
| D-Travel speed | 2710.88 | 2 | 1355.44 | 24.49 | 0.0026 | |
| AB | 12.96 | 1 | 12.96 | 0.2342 | 0.6489 | |
| AC | 2015.76 | 1 | 2015.76 | 36.42 | 0.0018 | |
| AD | 593.61 | 2 | 296.81 | 5.36 | 0.0570 | |
| BC | 15.76 | 1 | 15.76 | 0.2847 | 0.6165 | |
| BD | 280.07 | 2 | 140.04 | 2.53 | 0.1742 | |
| CD | 2397.72 | 2 | 1198.86 | 21.66 | 0.0034 | |
| $A^2$ | 1751.10 | 1 | 1751.10 | 31.63 | 0.0025 | |
| $B^2$ | 423.17 | 1 | 423.17 | 7.64 | 0.0396 | |
| $C^2$ | 85.75 | 1 | 85.75 | 1.55 | 0.2684 | |
| **Residual** | 276.77 | 5 | 55.35 | | | |
| Lack of Fit | 276.77 | 3 | 92.26 | | | |
| Pure Error | 0.0000 | 2 | 0.0000 | | | |
| **Cor Total** | 12810.87 | 22 | | | | |

The model's high F-value of 13.32 indicates that it is statistically significant, with a likelihood of 0.48% that the F-value is the result of random error. P-values ≤ 0.05 indicate that factors A, B, C, D, interactions AC and CD, and quadratic terms A2 and B2 significantly affect the answer. P-values greater than 0.1 indicate that the terms have no discernible effect on the forecasts. Streamlining the model by eliminating superfluous terms through stepwise selection may optimize it because some terms are extremely inconsequential. The ratio measuring signal versus noise preferred to be above 4; at 12.650, there is sufficient signal. Therefore, this validated model is reliable for navigating how the response behaves across the design space as conditions change. In conclusion, this analysis verifies the model appropriately describes the response based on the data.

### *3.3 Predicted and Actual Results for the three (3) Responses:*

#### *3.3.1 Weld bead geometry (width)*

The experimental design was enhanced through the utilization of Design Expert software. Formulated equations were generated for each specific scenario to predict anticipated experimental results.

A comparison between expected and observed results is shown graphically in Figure 2. In the context of the weld bead geometry (width) analysis, the graphical representation demonstrates a noteworthy resemblance between the predicted and observed values. Table 6 presents a systematic arrangement of the tabulated actual and expected data for the weld bead geometry (width) related to welding performance. This serves to validate that the experimental design and formulated equations effectively replicated the experimental findings.

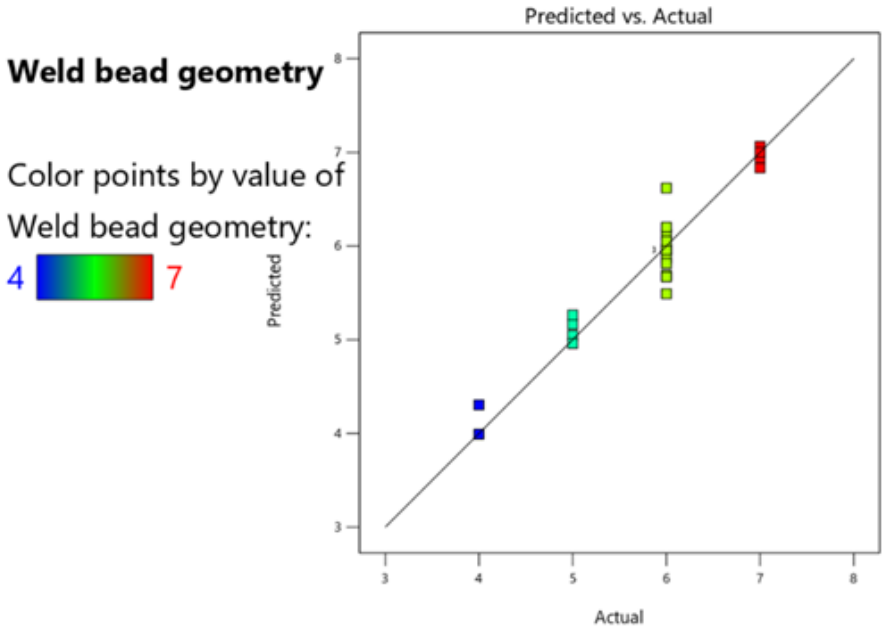


Figure 2: Showing the graphical representation of the predicted and actual values for Weld bead geometry (width)

Table 6: Showing the actual and predicted data sets of the weld bead geometry (width)

| Run Order | Actual Value | Predicted Value | Residual | Leverage | Internally Studentized Residuals | Externally Studentized Residuals | Cook's Distance | Influence on Fitted Value DFFITS | Standard Order |
|---|---|---|---|---|---|---|---|---|---|
| 1 | 5.00 | 5.27 | -0.2653 | 0.905 | -1.768 | -2.581 | 1.661(1) | -7.984(1) | 14 |
| 2 | 5.00 | 4.96 | 0.0396 | 0.977 | 0.533 | 0.491 | 0.662 | 3.179(1) | 21 |
| 3 | 6.00 | 5.87 | 0.1284 | 0.919 | 0.923 | 0.907 | 0.536 | 3.050(1) | 7 |
| 4 | 4.00 | 3.99 | 0.0074 | 0.964 | 0.080 | 0.072 | 0.010 | 0.373 | 16 |
| 5 | 4.00 | 4.31 | -0.3054 | 0.858 | -1.663 | -2.225 | 0.931 | -5.477(1) | 9 |
| 6 | 6.00 | 5.82 | 0.1840 | 0.824 | 0.899 | 0.878 | 0.210 | 1.901 | 11 |
| 7 | 6.00 | 6.62 | -0.6196 | 0.619 | -2.057 | -4.687 | 0.382 | -5.972(1) | 4 |
| 8 | 6.00 | 6.20 | -0.2022 | 0.873 | -1.164 | -1.220 | 0.520 | -3.204(1) | 3 |
| 9 | 6.00 | 5.96 | 0.0407 | 0.331 | 0.102 | 0.091 | 0.000 | 0.064 | 18 |
| 10 | 7.00 | 7.00 | 0.0014 | 0.933 | 0.011 | 0.010 | 0.000 | 0.037 | 6 |
| 11 | 6.00 | 5.49 | 0.5089 | 0.738 | 2.038 | 4.424 | 0.650 | 7.427(1) | 1 |
| 12 | 6.00 | 6.05 | -0.0530 | 0.991 | -1.142 | -1.188 | 7.952(1) | -12.446(1) | 20 |
| 13 | 7.00 | 7.00 | -0.0033 | 0.949 | -0.030 | -0.027 | 0.001 | -0.115 | 23 |
| 14 | 6.00 | 5.96 | 0.0407 | 0.331 | 0.102 | 0.091 | 0.000 | 0.064 | 19 |
| 15 | 7.00 | 6.84 | 0.1644 | 0.880 | 0.971 | 0.964 | 0.383 | 2.606 | 13 |
| 16 | 6.00 | 6.12 | -0.1249 | 0.533 | -0.375 | -0.340 | 0.009 | -0.364 | 2 |
| 17 | 6.00 | 5.69 | 0.3081 | 0.842 | 1.587 | 2.016 | 0.745 | 4.650(1) | 5 |
| 18 | 7.00 | 7.07 | -0.0652 | 0.988 | -1.209 | -1.285 | 6.575(1) | -11.567(1) | 22 |
| 19 | 5.00 | 5.17 | -0.1657 | 0.659 | -0.582 | -0.539 | 0.036 | -0.750 | 8 |
| 20 | 6.00 | 5.67 | 0.3297 | 0.773 | 1.419 | 1.643 | 0.382 | 3.036(1) | 10 |
| 21 | 6.00 | 5.96 | 0.0407 | 0.331 | 0.102 | 0.091 | 0.000 | 0.064 | 17 |
| 22 | 7.00 | 6.94 | 0.0583 | 0.815 | 0.278 | 0.251 | 0.019 | 0.527 | 12 |
| 23 | 5.00 | 5.05 | -0.0477 | 0.967 | -0.541 | -0.498 | 0.480 | -2.709(1) | 15 |

### *3.3.2 Microhardness values*

The actual and projected results of the experimental measurement of the microhardness magnitudes are graphically contrasted in Figure 3. Again, the graph shows a strong similarity between the expected and actual magnitudes, especially for this experiment. Table 7 contains the exact datasets that include both the actual and predicted data from the physical examinations about machine effectiveness. This table provides a thorough perspective on the trial's findings and ramifications, making it a useful point of reference. It makes it possible to compare the anticipated and actual magnitudes obtained. This result can be compared with that of Braide *et al.* [2022]

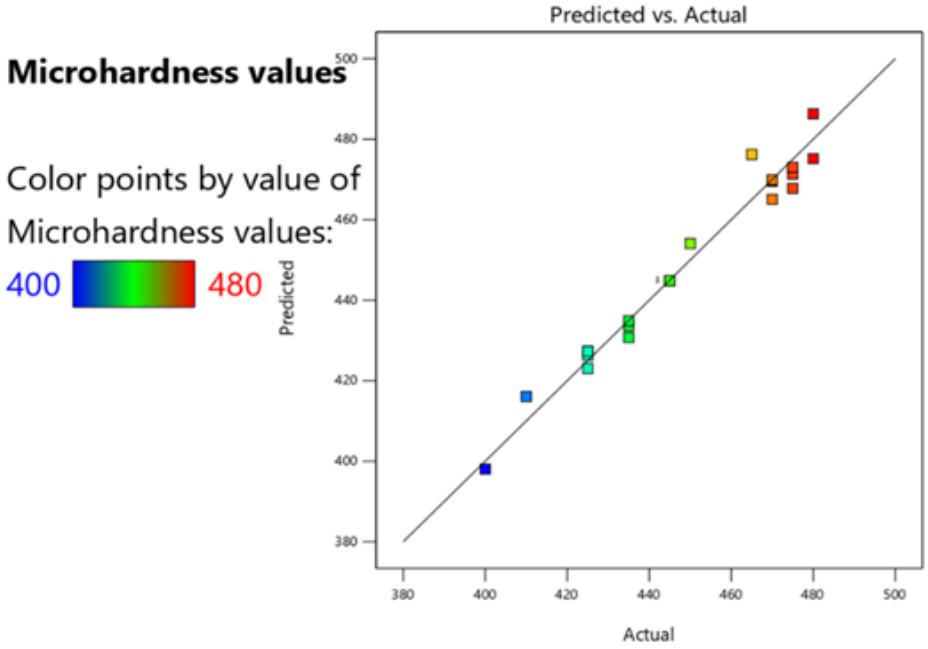


Figure 3: Showing the graphical representation of the predicted and actual values for Microhardness values

| Run Order | Actual Value | Predicted Value | Residual | Leverage | Internally Studentized Residuals | Externally Studentized Residuals | Cook's Distance | Influence on Fitted Value DFFITS | Standard Order |
|---|---|---|---|---|---|---|---|---|---|
| 1 | 450.00 | 454.07 | -4.07 | 0.905 | -1.524 | -1.863 | 1.235(1) | -5.763(1) | 14 |
| 2 | 425.00 | 423.04 | 1.96 | 0.977 | 1.479 | 1.763 | 5.103(1) | 11.428(1) | 21 |
| 3 | 475.00 | 471.33 | 3.67 | 0.919 | 1.484 | 1.774 | 1.384(1) | 5.968(1) | 7 |
| 4 | 400.00 | 398.03 | 1.97 | 0.964 | 1.197 | 1.267 | 2.145(1) | 6.580(1) | 16 |
| 5 | 410.00 | 416.05 | -6.05 | 0.858 | -1.852 | -2.956 | 1.155(1) | -7.277(1) | 9 |
| 6 | 435.00 | 430.72 | 4.28 | 0.824 | 1.175 | 1.235 | 0.359 | 2.674(1) | 11 |
| 7 | 465.00 | 476.21 | -11.21 | 0.619 | -2.091 | -5.281 | 0.394 | -6.729(1) | 4 |
| 8 | 480.00 | 486.32 | -6.32 | 0.873 | -2.046 | -4.533 | 1.604(1) | -11.906(1) | 3 |
| 9 | 445.00 | 444.83 | 0.1689 | 0.331 | 0.024 | 0.021 | 0.000 | 0.015 | 18 |
| 10 | 470.00 | 469.56 | 0.4372 | 0.933 | 0.194 | 0.175 | 0.029 | 0.651 | 6 |
| 11 | 475.00 | 467.77 | 7.23 | 0.738 | 1.628 | 2.124 | 0.415 | 3.565(1) | 1 |
| 12 | 435.00 | 434.88 | 0.1190 | 0.991 | 0.144 | 0.129 | 0.127 | 1.354 | 20 |
| 13 | 425.00 | 427.29 | -2.29 | 0.949 | -1.162 | -1.217 | 1.385(1) | -5.227(1) | 23 |
| 14 | 445.00 | 444.83 | 0.1689 | 0.331 | 0.024 | 0.021 | 0.000 | 0.015 | 19 |
| 15 | 470.00 | 469.78 | 0.2239 | 0.880 | 0.074 | 0.067 | 0.002 | 0.180 | 13 |
| 16 | 480.00 | 475.16 | 4.84 | 0.533 | 0.816 | 0.784 | 0.042 | 0.838 | 2 |
| 17 | 435.00 | 433.65 | 1.35 | 0.842 | 0.391 | 0.355 | 0.045 | 0.819 | 5 |
| 18 | 470.00 | 469.93 | 0.0683 | 0.988 | 0.071 | 0.064 | 0.023 | 0.574 | 22 |
| 19 | 425.00 | 426.31 | -1.31 | 0.659 | -0.258 | -0.232 | 0.007 | -0.323 | 8 |
| 20 | 475.00 | 473.03 | 1.97 | 0.773 | 0.477 | 0.436 | 0.043 | 0.806 | 10 |
| 21 | 445.00 | 444.83 | 0.1689 | 0.331 | 0.024 | 0.021 | 0.000 | 0.015 | 17 |
| 22 | 470.00 | 465.05 | 4.95 | 0.815 | 1.327 | 1.475 | 0.432 | 3.098(1) | 12 |
| 23 | 425.00 | 427.33 | -2.33 | 0.967 | -1.483 | -1.773 | 3.611(1) | -9.637(1) | 15 |

### *3.4 Effect of the investigated SMAW welding machine parameters on the Response:*

#### *3.4.1 Weld bead geometry (width)*

A contour graphic showing the relationship between four machine parameters: current (A), voltage (B), electrode diameter (C), travel speed (D), and weld bead shape (width) is shown in Figure 4. A deep interaction between current and voltage in relation to bead width is revealed by the contour graph. According to the data, the welding bead width grows as the welding machine's current and voltage rise. More specifically, the results imply that a greater machine voltage works better for the machine with respect to the geometry of the weld beads. In other words, the contour diagram illustrates the relationship between increasing the voltage and improving the welding machine's performance.

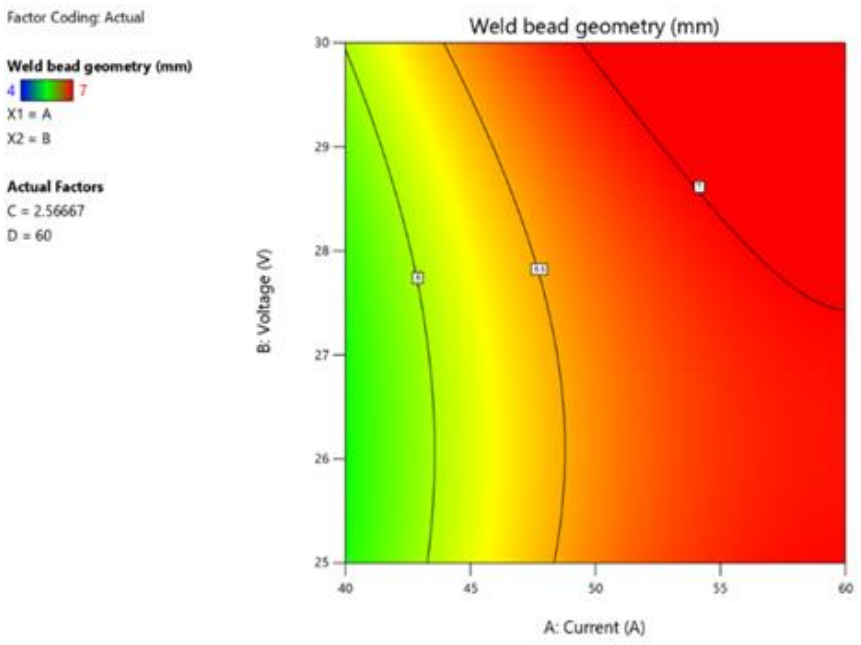


Figure 4: Contour plots of the response (Weld bead geometry (width) mm)

### *3.4.2 Microhardness values*

Once more, Figure .5 demonstrates a contour plot portraying the association among four machine variables: Current (A), Voltage (B), Electrode diameter (C), Travel speed (D), and Microhardness measurements. The contour plot reveals a significant interaction between current and voltage in relation to microhardness values. The data suggests that as the current of the welding apparatus increases and the voltage rises, there is an increase in the hardness values at a small scale. More specifically, the results propose that the machine operates more efficiently concerning hardness values when the machine voltage is elevated. In other words, augmenting the voltage results in improved performance of the welding equipment, as evidenced by the relationship depicted in the contour plot.

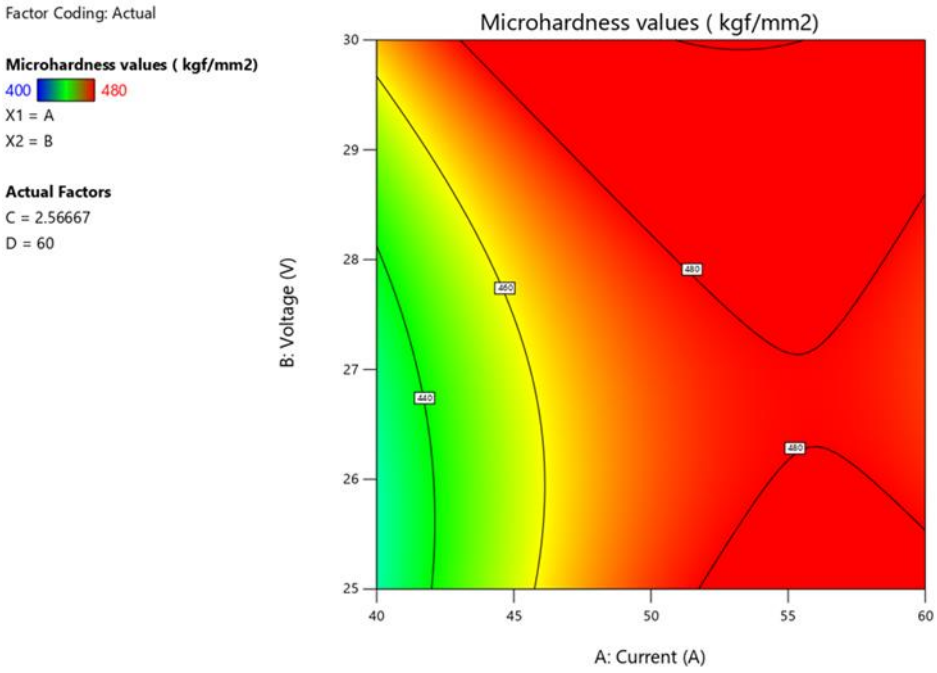


Figure 5: Contour plots of the response (Microhardness values)

### *3.4.3 Tensile shear strength*

A contour plot showing the relationship between four machine variables: current (A), voltage (B), electrode diameter (C), travel speed (D), and tensile shear strength values is once more shown in Figure 6. The contour plot indicates a noteworthy interplay between electrode diameter and current with respect to the value of tensile shear strength. According to the findings, the tensile shear strength values grow as the welding apparatus's current and electrode diameter increase. More precisely, the findings suggest that increasing the machine current and electrode diameter improves the tensile shear strength of a welded material. In other words, as the relationship illustrates, increasing the current leads to better welding equipment performance.

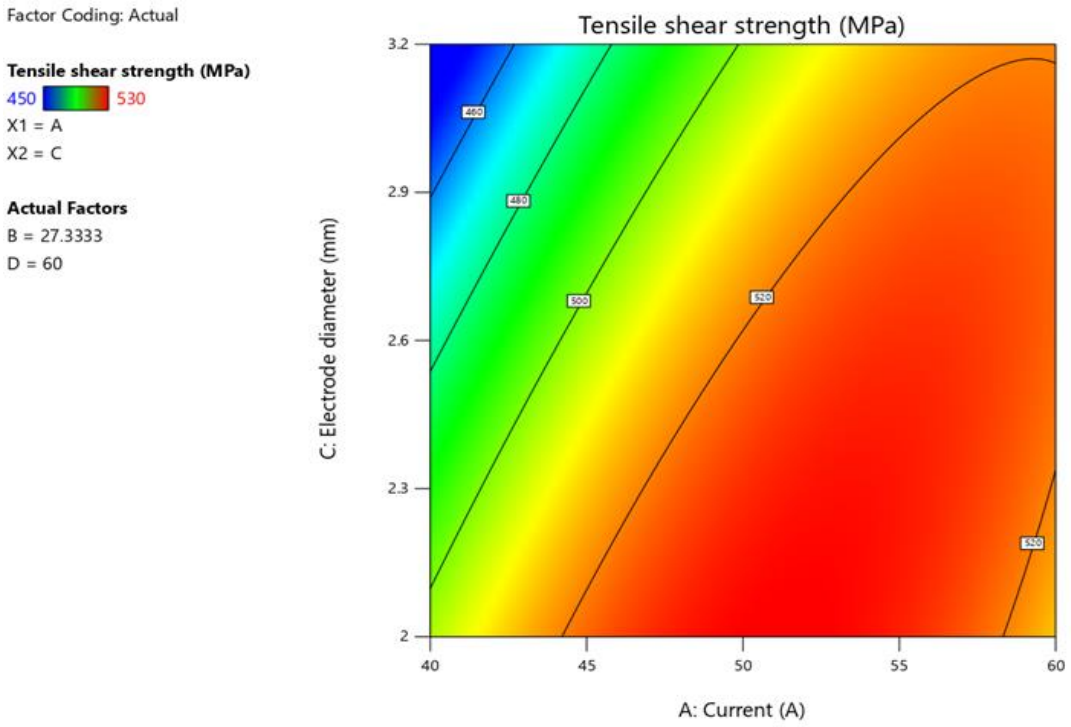


Figure 6: Contour plots of the response (Tensile shear strength)

### *3.4.4 Desirability Plot*

The ideal values found to yield the greatest results by combining the four categorical factor levels were travel speed of 100, voltage of 28.662, electrode diameter of 2.920, and current of 46.498. A bead width of 6.124 mm, a microhardness value of 437.736 kgf/mm2, and a tensile shear strength of 502.362 MPa are the anticipated results at these levels. In other words, according to the statistical modeling done, the maximum bead width and the highest microhardness and tensile strength values should be obtained by operating the welding process at the designated levels for each factor.

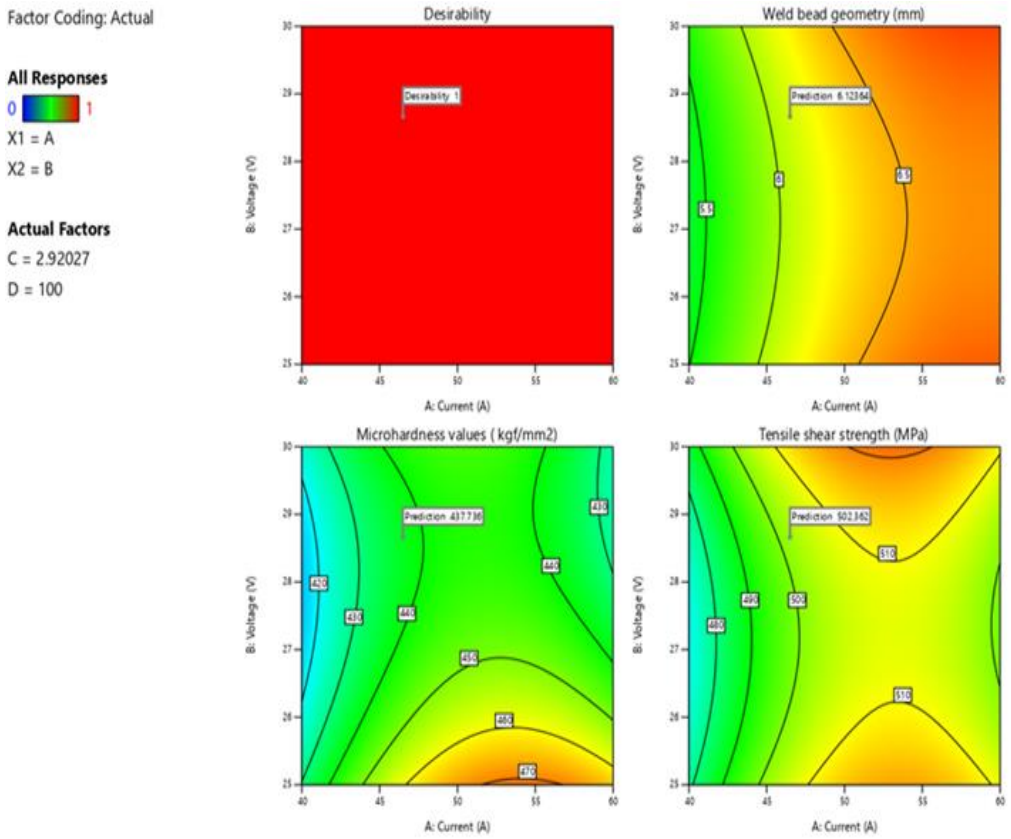


**Figure 7: Optimal Desirability plot**

## 4. Conclusions

The goal of this study was to use a locally manufactured arc welding machine to optimize the process parameters for welding ASTM A36 steel. In the course of the study, the following new information and conclusions are made:

1. The following parameter values resulted in welds with the highest microhardness value of 437.736 kgf/mm2, the narrowest bead width of 6.124 mm, and the greatest tensile shear strength of 502.362 MPa: 46.498 amps of current, 28.662 volts, electrode diameter of 2.920 mm, and travel speed of 100 mm/min. It was discovered that welding at these carefully calibrated settings far outperformed the machine's initial unregulated capability.
2. Remarkably, fewer errors needing expensive rework resulted in a productivity boost of nearly 25%. This clearly addressed one of the most important constraints facing small welding operations. Higher quality welds with better and more constant mechanical qualities may be consistently produced because of the optimized parameters. These increases were validated by statistical regression modeling during analysis, which predicted responses that were quite close to the measured values.
3. Although extremely positive results were achieved, several restrictions persisted. Variations may exist for welding various material thicknesses that merit further investigation, as the parameter optimization was done especially for 3mm thick steel plates. Furthermore, despite changing the parameters, the manual SMAW machine's maximum output power limited its use to a specific material thickness.
4. However, by creating best practices and benchmark methods for optimizing capability from available equipment resources, the knowledge gathered from this research significantly and sustainably increased local welding skills. The study's main goal was achieved thanks to the improved process comprehension and measurable advancements.

**Author contribution:** All the authors contributed to the development of the work.

**Data availability:** The authors confirm that the data supporting the findings of this study are available within the article.
**Declarations:** Ethics approval and consent to participate. This work does not include human and animal and hence does not require ethical approval from any committee and does not require consent to participate in the research.
**Consent for publication:** The authors give the publisher the consent to publish the work.
**Informed consent:** The work does not require informed consent in the research.
**Competing interests:** The authors declare no competing interests.

## References


[1] Braide T.T., Nwobi-Okoye C.C., and Ezechukwu V.C. (2022) Microstructural and Electrochemical study of Value-added Al-Si-Mg alloy reinforced with synthesis carbon nanotube and periwinkle shell nanoparticles for brake disc application, Chemical Data Collections, 39, 2022, 100878, ISSN 2405-8300, https://doi.org/10.1016/j.cdc.2022.100878. (https://www.sciencedirect.com/science/article/pii/S2405830022000519)

[2] Braide T. K, Chidozie C N, Vincent C E and Remy U. (2023) Multi objective optimization of novel Al-Si-Mg nanocomposites: A Taguchi-ANN-NSGA-II Approach, *Journal of Engineering Research,* 2023, ISSN 2307-1877, https://doi.org/10.1016/j.jer.2023.10.008. (https://www.sciencedirect.com/science/article/pii/S2307187723002687)

[3] Chidambaresh, S, Radhika, N., Deepak k N H, & Bal, S. (2023). A review on welding techniques: properties, characterisations, and engineering applications. Advances in Materials and Processing Technologies. 10. 1-56. 10.1080/2374068X.2023.2186638.

[4] Elahi, M., Afolaranmi, S.O. and Martinez L, J.L. et al. (2023) A comprehensive literature review of the applications of AI techniques through the lifecycle of industrial equipment. Discov Artif Intell 3, 43 (2023). https://doi.org/10.1007/s44163-023-00089-x

[5] Ezechukwu, V.C., Nwobi-Okoye, C.C. & Atanmo, P.N. (2020) Surface modification of Momordica angustisepala fiber using temperature-activated amino-functionalized alkali-silane treatment. Int J Adv Manuf Technol 109, 1397–1407 (2020). https://doi.org/10.1007/s00170-020-05697-w

[6] Ezechukwu, V.C., Nwobi-Okoye, C.C., Atanmo, P.N., Aigbodion, V.S. (2020). Wear performance of value-addition epoxy/breadfruit seed shell ash particles and functionalized Momordica angustisepala fiber hybrid composites. Revue des Composites et des Matériaux Avancés-*Journal of Composite and Advanced Materials,* 30, 5-6, 195-202. https://doi.org/10.18280/rcma.305-601

[7] Ezechukwu, V, C. (2024). Hybridization Effect on Thermo-mechanical Behaviour of Epoxy/breadfruit Seed Shell Ash Particles and Momordica Angustisepala Fiber Composites for High- temperature Devices Application. Proceedings of the IRE. 7. 2456-8880. https://www.irejournals.com/formatedpaper/1705783.pdf

[8] Ezechukwu V. E., Nwobi-Okoye C. C., and Onyenanu I. U. (2015) Analysis of Waste Gases at INTAFACT Beverages, Onitsha – Nigeria. *International Journal of Emerging Technologies and Innovative Research* (www.jetir.org), ISSN:2349-5162, 2, 10, page no.141-145, https://www.jetir.org/view?paper=JETIR1510026

[9] Erebugha, Y., Kennedy, C. and Ezechukwu, V.C. (2024). Green Plants Extracts Corrosion Inhibition of Aluminum -*A Review. Iconic Research and Engineering Journal (IRE)7*. 8-15. ISSN:2456-8880

[10] Martínez-Conesa, E & Egea, J A, Miguel, V, Toledo, C & Meseguer-Valdenebro, J. (2017). Optimization of geometric parameters in a welded joint through response surface methodology. Construction and Building Materials. 154. 105-114. 10.1016/j.conbuildmat.2017.07.163.

[11] Vietanti, F, Rajan, A, Arifin, A A, Feryanto, D, S, Hery U, Miftahul A, R & Dicky, M, and Darmawan, F. (2021). Analysis of Welding Position and Current on Mechanical Properties of A36 Steel using Shield Metal Arc Welding. *Journal of Physics: Conference Series*. 2117. 012001. 10.1088/1742-6596/2117/1/012001.